Chemical Geology
November 2020, Volume 555, Pages 119832 (13p.)
https://doi.org/10.1016/j.chemgeo.2020.119832
https://archimer.ifremer.fr/doc/00643/75496/

Microbial utilization of rare earth elements at cold seeps related to aerobic methane oxidation

Bayon Germain [1, *], Lemaitre Nolwenn [2], Barrat Jean-Alix [3], Wang Xudong [1, 4], Feng Dong [4], Duperron Sebastien [5, 6]

[1] IFREMER, Marine Geosciences Unit, 29280 Plouzané, France
[2] Institute of Geochemistry and Petrology, Department of Earth Sciences, ETH Zurich, CH-8092 Zurich, Switzerland
[3] Laboratoire Géosciences Océan, Université de Bretagne Occidentale et Institut Universitaire Européen de la Mer, 29280 Plouzané, France
[4] Shanghai Engineering Research Center of Hadal Science and Technology, College of Marine Sciences, Shanghai Ocean University, Shanghai 201306, China
[5] Muséum national d'Histoire naturelle–UMR7245 (MNHN CNRS) Mécanismes de Communication et Adaptation des Micro-organismes (MCAM), 75005 Paris, France
[6] Institut Universitaire de France, Paris, France

* Corresponding author : Germain Bayon, email address : gbayon@ifremer.fr

Abstract :

A major breakthrough in the field of rare earth element (REE) geochemistry has been the recent discovery of their utility to microbial life, as essential metalloenzymes catalyzing the oxidation of methanol to formaldehyde. Lanthanide-dependent bacteria are thought to be ubiquitous in marine and terrestrial environments, but direct field evidence of preferential microbial utilization of REE in natural systems is still lacking. In this study, we report on the REE and trace element composition of the tube of a siboglinid worm collected at a methane seep in the Gulf of Guinea; a tube-dwelling annelid that thrives in deep-sea chemosynthetic ecosystems. High-resolution trace element profiles along the chitin tube indicate marked enrichments of lanthanum (La) and cerium (Ce) in its oxic part, resulting in REE distribution patterns that depart significantly from the ambient seawater signature. Combined with various geochemical and microbiological evidence, this observation provides direct support for an active consumption of light-REE at cold seeps, associated with the aerobic microbial oxidation of methane. To further evaluate this hypothesis, we also re-examine the available set of REE data for modern seep carbonates worldwide. While most carbonate concretions at cold seeps generally display REE distribution patterns very similar to those for reduced pore waters in marine sediments, we find that seafloor carbonate pavements composed of aragonite commonly exhibit pronounced light-REE enrichments, as inferred from high shale-normalized La/Gd ratio (>~0.8), interpreted here as possibly reflecting the signature of lanthanide-dependent methanotrophic activity. This finding opens new perspectives for revisiting REE systematics in ancient seep carbonates and other microbialites throughout the Earth's history. In particular, the geochemical imprint of aerobic methane oxidation could be possibly traced using REE in Archaean stromatolites and other archives of Precambrian seawater chemistry, potentially providing new insights into the oxygenation of early Earth's oceans and associated microbiogeochemical processes.

Keywords : tubeworms, Siboglinidae, Lanthanide-dependent bacteria, metalloenzymes, methylotrophy, Regab, authigenic carbonates, Archaean

1. Introduction

Trace elements have long been known for their utility to biological systems, playing key roles in metalloenzymes that mediate important biochemical reactions (*e.g.*, Bowen, 1966). To some extent, the lanthanides, or rare earth elements (REE), also share biologically relevant properties (Tyler, 2004). For instance, they are thought to stimulate plant growth when added as fertilisers in agriculture (Tyler, 2004). However, compared to iron and other well-known essential metals, the biological role of REE still remains largely unexplored and poorly understood (Skrovan and Martinez-Gomez, 2015). A few years ago, a series of experimental works showed that microorganisms involved in the aerobic oxidation of methane were strongly dependent upon REE availability (*e.g.*, Fitriyanto et al., 2011; Nakagawa et al., 2012; Pol et al., 2014), demonstrating that light-REE (LREE), especially lanthanum (La) and cerium (Ce), were playing an active role as cofactors in a particular type (XoxF) of methanol dehydrogenase; a quinoprotein that catalyses the conversion of methanol to formaldehyde. Importantly, follow-up studies revealed that REE-dependent bacteria were probably ubiquitous in both marine and terrestrial environments (Taubert et al., 2015; Ochsner et al., 2019; Picone and Op den Camp, 2019). In a study that investigated the massive gas plume released to the Gulf of Mexico during the *Deepwater Horizon* blowout, Shiller et al. (2017) even proposed that aerobic methanotrophy could play a previously unrecognized role in the marine geochemical cycle of the REE, acting as a net sink for dissolved LREE in seawater. More recently, in a companion paper, we have reported the first documented evidence for methanotrophy-driven La enrichments in cold seep mussels from the South China Sea, both in the carbonate shells and associated soft tissues (Wang et al., 2020). A major finding of that work was the discovery that thiotrophic bivalves from the same sites (i.e. associated with sulphur-oxidizing bacteria) did not display any particular LREE enrichments, hence clearly suggesting that their occurrence in chemosynthetic mussels was solely related to lanthanide-

dependent methanotrophy. To date, this latter study represents the only field evidence for preferential REE utilization during methane oxidation processes in the marine environment. Additional work is needed to clarify the mechanism by which REE may be consumed by microbial activity in methane-rich environments, but also to assess whether authigenic carbonates and other geological archives of past fluid seepage may provide a record for REE-dependent methanotrophy.

Siboglinid tubeworms are ubiquitous chemosynthetic organisms at deep-sea hydrocarbon seeps and hydrocarbon vents (*e.g.*, Sibuet and Olu, 1998; Bright and Lallier, 2010), where they form large colonies (or 'bushes') at the seafloor, growing on hard substrates (Fig. 1a). For nutrition, siboglinid annelids rely entirely on internal suphide-oxidizing bacterial symbionts, which are hosted within specialized cells in a specific organ called the trophosome (*e.g.*, Boetius, 2005). At seeps, the required supply of sulphide comes from the underlying anoxic sediment (via anaerobic oxidation of methane or AOM; $CH_4 + SO_4^{2-} \rightarrow HCO_3^- + HS^- + H_2O$), where the posterior extension of the tube is rooted, often anchored into carbonates, but also, to a lesser extent, from the anterior fraction of the tube, thanks to in-tube water circulation (Julian et al., 1999; Cordes et al., 2005). In contrast, oxygen is acquired exclusively from overlying bottom waters at the anterior end of the animal via a large branchial plume (*e.g.*, Freytag et al., 2001). Siboglinid tubes also act as a direct conduit for seawater sulphate down to the buried posterior extension within the anoxic sediment (*e.g.*, Cordes et al., 2005). This process further promotes AOM and subsequent *in situ* production of dissolved sulphide that can be used as an additional source of energy for the internal symbionts. Within the animal, both dissolved sulphide and oxygen are co-transported by a specialized haemoglobin through the circulatory system to the trophosome (Flores et al., 2005). Siboglinid tubes are composed of chitin crystallites embedded in a protein matrix

(Gaill et al., 1992), but also host abundant and diverse microbial communities, including aerobic methane-oxidizing bacteria (Duperron et al., 2009; Medina-Silva et al., 2018). As such, the chitin-rich tube of siboglinid worms represents an ideal archive for investigating the links between trace elements and microbial activity at methane seeps and, in particular, to test the hypothesis that aerobic oxidation of methane can result in the preferential microbial utilization of light-REE.

In this study, we report REE and other trace element abundances along the tube of one specimen of *Escarpia southwardae*; a tubeworm from the annelid family Siboglinidae that is encountered in West African cold seeps (Andersen et al., 2004). This study builds upon an earlier investigation of the same tubeworm, which combined the characterization of the bacterial symbionts together with preliminary geochemical analyses (Mn, Fe, Sr, Zr) of the chitin tube (Duperron et al., 2014). The new REE data reported here are found to display major fluctuations along the tube, reflecting the combination of various factors, such as the presence of detrital particles embedded within the tube matrix, changes in the relative contribution of anoxic pore water versus oxic seawater, but also, importantly, the preferential utilization of La and other light-REE due to the aerobic oxidation of methane.

2. Material and methods

2.1. Study area and sample preparation

The studied siboglinid tube was collected by remotely operated vehicle (ROV) at the Regab cold seep using a hydraulically actuated Bushmaster device (5.798°S, 9.711°E; 3152 m water depth; Fig. 1a). Regab is a ~800 m wide giant pockmark at the Western African margin, characterized by intense methane seepage and the occurrence of gas hydrates,

massive carbonate deposits, and abundant chemosynthetic communities at the seafloor (*e.g.*, Charlou et al., 2004; Ondréas et al., 2005; Olu-Leroy et al., 2007; Pop Ristova et al., 2012; Marcon et al., 2014; Lemaitre et al., 2014). Upon recovery, the ~1-m-long chitinous tube was cut in sections perpendicular to the length of the tube, with sections S1 and S55 corresponding to the most anterior and posterior parts of the tube, respectively (Fig. 1b). All tube samples were cleaned with ultrapure water in ultrasonic bath prior to being digested with twice sub-boiled concentrated HNO_3.

2.32. Background information on the growth of siboglinid tubeworms and associated redox processes

Siboglinid tubeworms include some of the longest-lived animals on earth, with life spans extending up to 300 yr old (*e.g.*, Bergquist et al., 2000; Durkin et al., 2017). While the mode of growth of siboglinid tubeworms still remains poorly constrained, it is generally assumed that the tube can grow at both ends (*e.g.*, Gaill et al., 1997), resulting in the formation of successive concentric growth lines in the anterior extension of the tube that is bathed by ambient bottom waters. In situ growth measurements suggest that the tube of siboglinid annelids grows at an average rate of ~1 cm/yr (*e.g.* Bergquist et al., 2000; Cordes et al., 2005; Cordes et al., 2007; Durkin et al., 2017). The chitin-producing glands are located in the anterior end of the animal, associated with a muscular organ called the vestimentum (*e.g.*, Bright and Lallier, 2010). Several studies have suggested that chitin and protein dissolution may occur in the basal part of the animal due to secretion of enzymes (*e.g.*, Gaill et al., 1997).

At cold seeps, all species of siboglinid worms share a common habitat, living at the redox interface between oxic bottom waters and the reduced sediment. As mentioned above, a

preliminary set of data (Fe, Mn, Zr, Sr) has been already reported for the same tube of *Escarpia southwardae* investigated in this study (Duperron et al., 2014), indicating the presence of two distinct oxidation fronts along the tube. As inferred from Mn and Fe concentrations (Fig. 2), a first redox front was shown to occur near the posterior root-like extension of the tube (between sections S45-S49), corresponding to the redox interface between oxic bottom waters and the anoxic sediment. In marine sediments, early diagenetic processes proceed with the reduction of hydrogenous Fe-Mn oxyhydroxide phases under oxygen-depleted conditions (*e.g.*, Burdige, 1993). In organic-rich sediments or in areas influenced by methane seepage, this process typically occurs within the first tens of centimetres below the seafloor, releasing dissolved Mn^{2+} and Fe^{2+} into the surrounding pore waters, which then diffuse upwards until they re-precipitate as diagenetic Fe-Mn oxyhydroxides, when oxic conditions are met again near the seafloor or in bottom waters (*e.g.*, Burdige, 1993; Schulz et al., 1994; Bayon et al., 2011a; Pop-Ristova et al., 2012). A second oxidative front was also identified at the anterior end of the tube (S1-S8), inferred solely from Mn concentrations (Fig. 2) interpreted as the result of active oxygen uptake by the branchial plume (Duperron et al., 2014). As proposed in this latter study, intense oxygen consumption in the branchial plume region most likely result in a micro-redox gradient that could locally foster microbial activity, possibly playing a key role in the metabolism of siboniglids.

2.3. Methods

Concentrations for rare earth and other trace elements were determined at the Pôle Spectrométrie Océan (Brest, France) on an Element2 ICP-MS, after addition of a Tm spike and correction for polyatomic oxide and hydroxide interferences (Barrat et al., 1996). The precision and accuracy of our measurements were assessed by replicate analyses of the MA-

A-1/TM certified reference material (International Atomic Energy Agency; IAEA). MA-A-1 corresponds to homogenized copepods (*Calanus cristatus*) collected from the Norwegian Sea and composed of chitin. Precision (expressed as relative standard deviation in Table 1) was better than 15% RSD for most elements, except Zr (18.7%), Mo (24%), Gd (18.1%) and Th (15.8%). The accuracy of our procedure was evaluated by comparing our results to recommended values for V, Mn, Fe, Co, Ni, Cu and Zn (Table 1; International Atomic Energy Agency, 1990; Maher et al., 2001), demonstrating relatively good agreement (within 15%) except for V (24%). For other elements, the accuracy was assessed by analysing MA-A-1 after an additional step of iron oxide co-precipitation; a method that allows quantitative extraction of reactive trace elements (including REE) and separation from the sample matrix, resulting in accurate results for various geological samples (Bayon et al., 2009a; Bayon et al., 2011b). The good agreement obtained between the two datasets (Table 1) further validates our procedure for the following elements: Mn, Y, REE and Th. The REE concentrations were normalized to World River Average Silt (WRAS) abundances (Bayon et al., 2015). The La and Ce enrichments in studied sections of the tube were quantified using the shale-normalized ($_N$) La (La/La*) and (Ce/Ce*) anomalies, where La* and Ce* correspond to theoretical concentrations calculated geometrically assuming that the behaviour of their respective REE neighbours is linear on a log-linear plot (Lawrence et al., 2006), with $La^* = Pr_N \times (Pr_N/Nd_N)^2$ and $Ce^* = Pr_N \times (Pr_N/Nd_N)$, respectively. Positive and negative La and Ce anomalies are indicated by La/La* and Ce/Ce* > 1 and < 1, respectively.

3. Results

Measured trace element abundances in the tube sections are reported in Table 2. Selected elemental profiles for REE (La, Gd) and other trace elements (Mn, Fe, Th, V, Mo, U and Cu) along the tube are presented in Fig. 2. As previously shown for Fe and Zr (Duperron et al.,

2014), Th and other elements typically associated with the silicate detrital fraction of the sediment (*e.g.*, Rb, Ba) display marked enrichments in both anterior and posterior extensions of the tube (Fig. 2). The REE also display similar concentration profiles (*e.g.*, La, Gd; Fig. 2), with La abundances fluctuating over more than one order of magnitude between the anterior end of the tube (319 ng/g in section S1), to its middle (21 ng/g; S30) and posterior (417 ng/g; S55) parts. However, while high Gd abundances in the anterior portion of the tube mainly occur in sections S1 and S2, the observed La enrichment extends down to section S22 approximately, as clearly shown by higher $(La/Gd)_N$ in this portion of the tube (Fig. 2). Note that the La and Gd (and other REE) also exhibit a small enrichment at ~ 85 cm, similar to that previously observed for Mn and Fe (Duperron et al., 2014). Copper exhibits a slightly different profile along the tube, characterized by high concentrations in the anterior part (> 10 µg/g in sections S1-2) and a smooth decrease in the remaining part of the tube. Finally, the three redox sensitive elements (V, Mo and U) display markedly different elemental profiles along the tube, with their lowest concentrations being observed in the anterior extension of the tube (Fig. 2). Along the tube, V, Mo and U display similar trends until ~80 cm, characterized by a sudden increase of concentrations in the anterior part of the tube (*e.g.*, from ~ 0.2 to 10 µg/g for U), followed by a gentle decrease to reach minimum values between sections S22 and S44. Below the seawater-sediment interface (~80 cm), Mo and V abundances increase steadily, while U concentrations remain near constant (Fig. 2).

4. Discussion

4.1. U, Mo and V constraints on changing redox conditions along the tube

Our new set of data includes trace elements (V, Mo and U) that are more soluble in oxic environments than under oxygen-depleted conditions (for a detailed review of the behaviour of redox-sensitive elements in the marine environment, see Tribovillard et al., 2006 and

Smrzka et al., 2019). These redox elements are typically enriched in reduced organic-rich sediments, being relatively unaffected by the presence of detrital silicate minerals. As such, they are commonly used in sedimentary records as paleoproductivity and/or paleoredox proxies (*e.g.*, Algeo and Maynard, 2004; Tribovillard et al., 2006). In seepage areas, the presence of significant Mo and U enrichments in sub-surface sediment horizons has been also interpreted as reflecting fossil evidence for past circulation events of methane-rich fluids (Peketi et al., 2012; Sato et al., 2012; Hu et al., 2015; Chen et al., 2016). In the marine environment, both Mo and V share strong affinities with Mn oxides and, as a consequence, are strongly affected by the redox cycling of Mn at the seawater-sediment interface (*e.g.*, Calvert and Pedersen, 1993; Crusius et al., 1996). Under oxygen-depleted conditions, increasing levels of dissolved sulphide typically lead to enhanced sequestration of Mo and V into various organic compounds and sulphide minerals in the sediment (*e.g.*, Tribovillard et al., 2006). Unlike Mo and V, the enrichment of U in reduced marine sediments is not influenced by the redox cycling of Fe-Mn oxyhydroxides, nor does it reflect the levels of dissolved hydrogen sulphide in the surrounding environment (*e.g.*, Algeo and Maynard, 2004; McManus et al., 2005).

Based on the above, the steady increase of V, Mo and U concentrations starting from the most anterior part of the tube (i.e. the 'upper' 10 cm, between S1 and S8) is best explained as reflecting a sharp redox gradient between oxic bottom waters (where V, Mo and U are mostly present in soluble forms) and the branchial plume region associated with intense oxygen consumption (where oxygen-depleted conditions are expected to result in the preferential immobilization of these redox-sensitive elements). Due to their known affinity with Mn, it is also possible that some of the observed enrichments for V and Mo in this part of the tube also partly relate to the redox cycling of Mn. Between ~10 and 80 cm, the progressively

decreasing V and Mo concentrations along the tube (and to a lesser extent U) presumably reflect the presence of less reduced conditions, although the persistence of relatively high U concentrations in this portion of the tube may still point towards relatively low oxygen levels. Finally, in the posterior part of the tube rooted in the sediment, below ~80 cm, the sharp increase of Mo concentrations (and to a lesser extent V) most likely indicates the presence of high levels of dissolved sulphide below the seawater-sediment interface. Overall, the interpretations based on the use of these three redox-sensitive elements agree well with the hypothesis proposed earlier by Duperron et al. (2014), confirming that siboglinid tubes are associated with the presence of sharp redox gradients at both posterior and anterior extensions.

4.2. Pore water versus seawater REE signatures along the siboglinid tube

In sections S1 and S2, high La and other REE abundances are best explained by the presence of detrital particles embedded within the chitin-rich matrix, as inferred both from corresponding high contents of Th and other terrigenous elements (Fig. 2; Table 2) and relatively flat shale-normalized REE distribution patterns (Fig. 3a). This recently-secreted portion of the tube is indeed much thinner than the rest of the chitinous tube (except for its posterior root-like extension; Duperron et al., 2014), and hence most likely to be 'contaminated' with particles derived from ambient turbid bottom waters. Below the seawater-sediment interface (between S45-S55), the observed increasing REE abundances could also reflect to some extent the presence of detrital particles, but also, presumably, the acquisition by the chitin tube of dissolved REE from surrounding pore waters. At ocean margins, anoxic pore waters typically display mid-REE (MREE) enrichments and positive Ce anomalies as a result of the reductive dissolution of Fe-Mn oxyhydroxide phases (*e.g.*, Sholkovitz et al., 1989; Haley et al., 2004; Himmler et al., 2013; Abbott et al., 2015), with

corresponding distribution patterns that closely resemble those determined in the most posterior sections of *Escarpia southwardae* (Fig. 3d). Instead, the anterior part of the tube, located above the seawater-sediment interface, is characterized by REE distribution patterns exhibiting a progressive increase of heavy-REE relative to the LREE; a feature that is typical of seawater (Fig. 3d). This feature is most apparent in the portion of the tube located between sections S22-S44 (Fig. 3c), where REE exhibit shale-normalized signatures very similar to that of ambient seawater, including the presence of pronounced negative Ce anomalies (Lemaitre et al., 2014; see the red dotted line in Fig. 3d). Taken together, these characteristics indicate that ambient bottom waters most likely acted as the main source of dissolved REE in this portion of the tube.

The relative influence of pore water *versus* seawater REE signatures in the studied siboglinid tube can be further constrained using both Ce and La anomalies. Along the tube, Ce anomalies display a general trend from positive (> 1) to negative (< 1) Ce/Ce* values from its apical end to ~ 75 cm, followed below the seawater-sediment interface, by a marked increase up to Ce/Ce* ~ 1.4 (Fig. 2). Except for the first two sections S1-S2, La anomalies display a similar depth-profile in the anterior part of the tube, characterized by a gradual decrease from high (~ 3-4) to low (~ 1-2) La/La* values (Fig. 2). However, in contrast to Ce/Ce*, La anomalies remain at low La/La* values (~ 1-2) below the seawater-sediment interface, except for two samples (S51 and S52). This decoupling between Ce and La anomalies can be also illustrated in a Ce/Ce* vs La/La* graph (Fig. 4), where our results for the tube sections are compared to an extensive compilation of literature data for pore waters and seawater (see Tables S1 and S2). Apart from sections S51 and S52, all the sections derived from the buried posterior extension of the tube clearly plot within the field defined by pore waters, while sections from the tube interval between sections S22 and S44 plot within the field of seawater.

This latter observation agrees well with the hypothesis that seawater actively circulates within the tube (Cordes et al, 2005; Duperron et al, 2014). In Fig. 4, the tube sections between S22 and S44 are aligned along a general mixing relationship defined by bottom waters at Regab, from both the seafloor (<1m elevation) and the overlying water column (>1m), and pore waters, which suggests that while ambient waters probably act as a major source of REE in the anterior part of the tube, their REE signature is also probably partially influenced by pore waters.

4.3. Evidence for microbial utilization of LREE related to aerobic oxidation of methane

A striking feature of Fig. 4 is that most sections from the most anterior part of the tube depart significantly from the 'seawater & pore water' array, displaying higher-than-normal La anomalies. Between S3 and S21, changing REE abundances are also reflected by flatter shale-normalized patterns and the absence of negative Ce anomalies (Fig. 3a,b), indicating that REE decoupling probably occurs along this section of the tube. It is unlikely that this change in shale-normalized patterns results from co-precipitation onto Mn oxyhydroxide phases, as could be possibly inferred from increasing Mn contents in the same part of the tube. If this was the case, one would expect similarly corresponding enrichments in trace elements such as Co, which generally share strong affinities for Mn oxides (Table 2). Additionally, any authigenic Mn-oxide phase associated with the chitin tube would be expected to display a shale-normalized REE pattern similar to that of anoxic pore waters, hence without any particular La anomalies. This is illustrated by the fact that leached Fe-Mn oxyhydroxide phases from surficial Congo Fan sediments (Bayon et al., 2004) plot well within the field of pore waters in Fig. 4. Instead, we propose below that the light-REE enrichments observed in the anterior portion of the tube could be related to microbial processes.

There is plentiful evidence that active microbial activity takes place in the anterior part of siboglinid tubes at cold seeps. For instance, recent studies conducted at methane seeps recently identified Methylococcales and other methanotrophic bacteria as an abundant microbial group in the anterior portion of chitin tubes of siboglinids, including *Escarpia southwardae* (Medina-Silva et al., 2018; Rincón-Tomás et al., 2020). In addition to the primary sulphur-oxidizing symbionts present in the animal itself, the presence of abundant methanotrophic bacteria in the upper part of the tube of a *Lamellibrachia* species was also supported using methanotroph-specific molecular probes and sequencing of a subunit of methane monooxygenase (Duperron et al., 2009). While the nutritional role of these tube-associated bacteria to their siboglinid hosts remains largely unknown (Hilario et al., 2011), all the above evidence collectively suggest that methanotrophs are common colonizers of the tubes of seep tubeworms worldwide, which could possibly contribute to the biomineralization of the tube (. Like other families of aerobic methane-oxidising bacteria, most Methylococcales possess both the methane monooxygenase (MMO) and methanol dehydrogenase (MDH) enzymes, which catalyse the oxidation of methane to methanol and subsequent conversion to formaldehyde, respectively (*e.g.*, Semrau et al., 2018). As mentioned in the Introduction, the activity of the XoxF-type of methanol dehydrogenase is now known to be strongly dependent on light-REE availability, especially La and Ce. Instead, the first step of methane oxidation is mostly controlled by copper availability. When Cu is abundant, methanotrophs express a membrane-bound Cu-containing enzyme called particulate methane monooxygenase (pMMO), which catalyzes the oxidation of methane to methanol (*e.g.*, Glass and Orphan, 2012). In the studied tube of *Escarpia southwardae*, the abundance profile for Cu closely follows that for La (Fig. 2). Additionally, Cu contents, after normalization to Th in order to correct from any effect related to the presence of detrital particles, also display strong positive relationships with both La/Th and shale-normalized La

anomaly (Fig. 5). To a lesser extent, Cu also shows positive correlations with Ce/Th ratios and Ce/Ce* in the anterior region of the studied tube, hence suggesting that these two elements are also involved in the same biogeochemical processes along the tube. While the magnitude of measured Ce anomalies along the studied tube is likely to be strongly influenced by various diagenetic processes (presence of Mn oxyhydroxide phases) and source effects (relative seawater *versus* pore water contributions), this observation is consistent with previous investigations, which suggested that both La and Ce can be transported and used at similar rates by methanotrophs and methylotrophs (e.g. Pol et al., 2014; Semrau, 2018; Daumann, 2019; Picone and Op den Camp, 2019). Therefore, in agreement with our recent findings on chemosynthetic mussels from the South China Sea (Wang et al., 2020), the above lines of evidence strongly suggest that the aerobic oxidation of methane at cold seeps can result in the combined uptake of both dissolved light-REE and Cu in the anterior extension of cold seep siboglinid tubes.

4.4. Revisiting REE systematics in modern cold seep carbonates

Unlike the Gulf of Mexico, where intense LREE scavenging had occurred in the water column following the *Deepwater Horizon* oil spill, no significant LREE depletion was identified in the bottom waters at Regab (Lemaitre et al., 2014). The massive amounts of methane accidentally released during the *Deepwater Horizon* disaster (Joye et al., 2011) possibly accounted for as much as a few percent of the total flux of natural CH_4 emitted from the seafloor at ocean margins annually (Boetius and Wenzhöfer, 2013), resulting locally in unprecedented high rates of methane oxidation into the water column (Crespo-Medina et al., 2014). Instead, at natural submarine seeps, *anaerobic* oxidation of methane represents an effective filter for CH_4 in the sediment (Boetius and Wenzhöfer, 2013), so that rates of *aerobic* methane oxidation in the overlying water column are consequently much reduced. At

Regab, the absence of any dissolved REE enrichment in bottom waters contrasted with the behaviour of Mn and Fe, which both displayed significantly higher dissolved contents in the water column overlying seepage sites (Lemaitre et al., 2014). This discrepancy between elements generally exhibiting relatively similar geochemical behaviour in the marine environment was interpreted as reflecting preferential removal of REE during precipitation of authigenic carbonates in sub-surface sediments (Lemaitre et al., 2014). In the light of our findings, future investigations should also investigate whether microbial REE uptake by chemosynthtic communities could also account, at least to some extent, for REE removal at cold seeps.

To further evaluate the hypothesis that aerobic methane oxidation can drive preferential utilization of LREE at submarine methane seeps, we also re-examine the available set of REE data for modern cold seep carbonates worldwide, which complements the recent literature review by Smrzka et al. (2020). At cold seeps, authigenic carbonates represent a direct by-product of the anaerobic pathway for methane oxidation (AOM), resulting from enhanced alkalinity and carbonate saturation levels in the surrounding pore waters (*e.g.*, Aloisi et al., 2002). The type and mineralogical composition of authigenic carbonates is strongly dependent upon the upward methane flux and the depth at which the AOM takes place within the sediment; the so-called sulphate-methane transition zone (SMTZ). In areas of high CH_4 fluxes, AOM typically proceeds near the seafloor, resulting in the formation of massive carbonate pavements dominated by aragonite and associated with abundant chemosynthetic fauna (*e.g.*, Greinert et al., 2001; Naehr et al., 2007). In contrast, in areas of reduced methane seepage, the depth of the SMTZ is encountered deeper within the sediment column (e.g., Borowski et al., 1996), where AOM and the presence of sulphate-depleted conditions are typically accompanied by the formation of homogeneous nodules of high-Mg carbonates,

such as high-Mg calcite, dolomite or siderite (*e.g.*, Aloisi et al., 2002; Gieskes et al., 2005; Bayon et al., 2007; Naehr et al., 2007). Despite of the genetic link between AOM and authigenic carbonates at cold seeps, the formation of aragonite at the seafloor has been occasionally associated with the presence of oxic conditions, at least locally, as inferred from the occurrence of negative Ce anomalies and various molecular fossils (biomarkers) of aerobic methanotrophic bacteria (*e.g.*, Birgel et al., 2011; Himmler et al., 2015). As such, seafloor carbonate pavements can represent potential archives for searching additional evidence of the preferential microbial utilization of LREE through aerobic methane oxidation.

In Fig. 6, we investigate the relationships between Ce/Ce* and La/La* in modern cold seep carbonates worldwide (Feng et al., 2008, 2009a, 2010; Himmler et al., 2010; Birgel et al., 2011; Rongemaille et al., 2011; Bayon et al., 2013; Hu et al., 2014; Pierre et al., 2014; Wang et al., 2014, 2015; Novikova et al., 2015; Crémière et al., 2016 ; Franchi et al., 2017 ; Yang et al., 2018; Smrzka et al., 2019 ; Wang et al., 2019). Note that all these literature data for modern seep carbonates are also compiled in Table S3. Authigenic carbonates were classified into two groups depending on their dominant mineralogy: aragonite and high-Mg carbonates. As expected, high-Mg carbonates clearly plot within the field of pore waters in Fig. 6a, yielding average La and Ce anomalies of 1.14 ± 0.30 and 1.09 ± 0.24 (1SD; n=160), respectively. Most aragonite crusts at cold seeps also plot in the field of pore waters, but exhibit slightly lower Ce anomalies (0.97 ± 0.31) and higher La/La* average values (1.21 ± 0.31; n=114). In Fig. 6a, a few aragonite samples associated with low Ce anomalies, hence displaying a seawater-like REE signature, also appear to exhibit slightly higher La anomalies (with La/La* > ~1.5). However, these values remain within the observed range of La/La* values in seawater (between ~ 1 and 3), so their interpretation in terms of preferential La microbial utilization cannot be conclusive.

In Fig. 6b, we also examine the relationships between shale-normalized La/Gd and Gd/Yb ratios in the same set of seep carbonate samples. As recently shown (Bayon et al., 2020), this graph is particularly well suited for investigating the general shape of shale-normalized REE patterns, especially for discriminating between samples exhibiting a typical MREE bulge of anoxic pore waters (characterized by relatively low $(La/Gd)_N$ and high $(Gd/Yb)_N$ values) and those displaying seawater-like patterns (characterized by both low $(La/Gd)_N$ and high $(Gd/Yb)_N$ values). In Fig. 6b, the observed range of $(La/Gd)_N$ and $(Gd/Yb)_N$ values in high-Mg carbonates also remarkably overlaps with pore water data. However, while most aragonite concretions do display similar $(La/Gd)_N$ and $(Gd/Yb)_N$ values, many of them appear to depart significantly from the fields defined by pore waters and seawater, being characterized by substantially higher shale-normalized La/Gd ratios (up to ~ 2.2; Fig. 6b). A similar observation can be drawn when plotting $(Pr/Gd)_N$ versus $(Gd/Yb)_N$ for the same set of authigenic carbonate samples (graph not shown here), indicating that these particular samples are also enriched in other LREE relative to the MREE.

A shared characteristic of those carbonate samples with high $(La/Gd)_N$ ratios is that they correspond to aragonite-rich seafloor carbonate pavements from the Gulf of Mexico (Feng et al., 2009a; Birgel et al., 2011; Hu et al., 2014; Smrzka et al., 2019), the Niger delta (Rongemaille et al., 2011, Wang et al., 2019), the Makran accretionary prism (Himmler et al., 2010), and the Mediterranean Sea (Franchi et al., 2017), which are all closely associated with abundant chemosynthetic fauna (*e.g.*, bathymodiolin mussels, tube worms) that live in symbiosis with aerobic methane-consuming microbes (*e.g.*, Aharon, 1994; Greinert et al., 2001; Teichert et al., 2005; Han et al., 2008). On this basis, the occurrence of anomalously high $(La/Gd)_N$ in chemoherm carbonates at cold seeps could possibly reflect the presence of shell fragments bearing the REE signature of the aerobic oxidation of methane. However, considering the recent REE data obtained on methanotrophic mussels from the South China

Sea (with a mean shale-normalized La/Gd ratio ~ 3.7; Wang et al., 2020), this hypothesis would be quite unlikely because REE concentrations in the carbonate shells are depleted by about two orders of magnitude compared to seep carbonates. In the Gulf of Mexico, the occurrence of pronounced LREE enrichments has been documented in laser-ablated aragonite phases from carbonate pavements associated with asphalt volcanism, interpreted as reflecting the degradation of liquid hydrocarbons (Smrzka et al., 2019; Fig. 6b). As proposed in that latter study, such LREE enrichments could be taken as diagnostic features for the influence of oil seepage at seep sites. Additionally, the presence of LREE enrichments in seafloor aragonite concretions could also reflect their close association with the chemosynthetic biomass, as proposed recently in an investigation of ancient seep carbonates by laser-ablation ICP-MS (Zwicker et al., 2018; Fig. 6b). At cold seeps, spectacular LREE enrichments have been indeed identified in the soft tissues of chemosynthetic mussels (with shale-normalized La/Gd ratios of up to ~ 100), which were clearly attributed to reflecting the signature of REE-dependent methanotrophy (Wang et al., 2020). Seafloor carbonate pavements are typically traversed by a dense network of tubular holes, which marks the presence of ancient siboglinid tubeworms whose tubes have now been dissolved (*e.g.*, Feng and Roberts, 2010; Feng et al., 2013). This process probably occurs over short timescales (a few decades or centuries) because recent carbonate crusts (as inferred from U-Th dating) commonly display the same petrographic features (*e.g.*, Bayon et al., 2009b). Based on the above, we suggest that the degradation of chitin tubes and/or other organic compounds bearing the geochemical signature of lanthanide-dependent methanotrophy could possibly result locally in the release of LREE-enriched dissolved signatures that would be subsequently incorporated into authigenic aragonite. Such a process could possibly account for some of the observed LREE enrichments in modern seep carbonates, in addition to providing a plausible explanation for

the presence of 'aerobic' geochemical signatures in authigenic carbonates formed otherwise via AOM.

5. Concluding remarks and future perspectives

Our high-resolution trace element investigation of a one-meter long chitin tube of a deep-sea siboglinid worm provides new evidence for the occurrence of aerobic microbial utilization of light-REE at cold seeps. In the branchial plume region of the tubeworm, the combined uptake of both Cu and LREE (especially La and Ce) from ambient seawater is inferred to be associated with the presence of tube-associated methane-consuming bacteria, serving as metalloenzymes for the transformation of methane to methanol, and subsequent conversion to formaldehyde, respectively. A reassessment of REE data for modern authigenic carbonates worldwide also suggests discernible signatures of lanthanide-dependent methanotrophy in many seafloor aragonite pavements, as inferred from the presence of anomalously high La contents compared to other REE (with shale-normalized La/Gd ratios > ~ 0.8). Such LREE enrichments in seep carbonates could possibly reflect the acquisition of geochemical signatures inherited from the degradation of chemosynthetic biomass supported by REE-dependent methanotrophy.

In future studies, we anticipate that these findings and their application to fossil microbial carbonates could provide new insights into the biogeochemical processes operating in ancient oceans. This could include the re-evaluation of previous REE datasets for ancient seep carbonates (*e.g.*, Feng et al., 2009b; Tong and Chen, 2012; Tribovillard et al., 2013; Della Porta et al., 2015; Colin et al., 2015; Smrzka et al., 2016; Zwicker et al., 2018; Argentino et al., 2019; Zhu et al., 2019), but also for various microbial archives of Precambrian oceans, at times when methane levels were presumably much higher both in the atmosphere and oceans (*e.g.*, Catling et al., 2001; Konhauser et al., 2009). For instance, many Late Archaean

stromatolites also display marked enrichments in La and other LREE (e.g., Kamber and Webb, 2001; Planavsky et al., 2010; Kamber et al., 2014; Schier et al., 2018). Future work could aim at investigating whether these particular features, generally taken as evidence for the presence of severely depleted oxygen levels in shallow waters (*e.g.*, Kamber et al., 2014), could also possibly correspond to the geochemical imprint of lanthanide-dependent methanotrophy in early Earth's oceans.

Acknowledgments

We thank the crews of R/V *Pourquoi Pas?* and all participants of the WACS cruise (2011; PI: Karine Olu-Leroy) for their assistance at sea. Claire Bassoulet is warmly acknowledged for assistance during ICPMS measurements. We also thank the Editor (Michael Boettcher), Tobias Himmler and two anonymous reviewers for providing insightful comments on this manuscript. This work was funded by IFREMER.

References

Abbott, A.N., Haley, B.A., McManus, J., Reimers, C.E., 2015. The sedimentary flux of dissolved rare earth elements to the ocean. Geochim. Cosmochim. Acta 154, 186-200.

Aharon, P., 1994. Geology and biology of modern and ancient submarine hydrocarbon seeps and vents: an introduction. Geo-Mar. Lett. 14, 69-73.

Algeo, T.J., Maynard, J.B., 2004. Trace-element behavior and redox facies in core shales of Upper Pennsylvanian Kansas-type cyclothems. Chem. Geol. 206, 289-318.

Aloisi, G., Bouloubassi, I., Heijs, S.K., Pancost, R.D., Pierre, C., Damsté, J.S.S., Gottschal, J.C., Forney, L.J., Rouchy, J. M., 2002. CH_4-consuming microorganisms and the formation of carbonate crusts at cold seeps. Earth Planet. Sci. Lett. 203, 195-203.

Andersen, A.C., Hourdez, S., Marie, B., Jollivet, D., Lallier, F.H., Sibuet, M., 2004. Escarpia southwardae sp. nov., a new species of vestimentiferan tubeworm (Annelida, Siboglinidae) from West African cold seeps. Canad. J. Zool. 82, 980-999.

Argentino, C., Lugli, F., Cipriani, A., Conti, S., Fontana, D., 2019. A deep fluid source of radiogenic Sr and highly dynamic seepage conditions recorded in Miocene seep carbonates of the northern Apennines (Italy). Chem. Geol. 522, 135-147.

Barrat, J.A., Keller, F., Amosse, J., Taylor, R.N., Nesbitt, R.W., Hirata, T., 1996. Determination of rare earth elements in sixteen silicate reference samples by ICP-MS after Tm addition and ion exchange separation. Geostand. Newslett. 20, 133-139.

Bayon, G., German, C.R., Burton, K.W., Nesbitt, R.W., Rogers, N., 2004. Sedimentary Fe–Mn oxyhydroxides as paleoceanographic archives and the role of aeolian flux in regulating oceanic dissolved REE. Earth Planet. Sci. Lett. 224, 477-492.

Bayon, G., Pierre, C., Etoubleau, J., Voisset, M., Cauquil, E., Marsset, T., Sultan, N., Le Drezen, E., Fouquet, Y., 2007. Sr/Ca and Mg/Ca ratios in Niger Delta sediments: implications for authigenic carbonate genesis in cold seep environments. Mar. Geol. 241, 93-109.

Bayon, G., Barrat, J.A., Etoubleau, J., Benoit, M., Bollinger, C., Révillon, S., 2009a. Determination of rare earth elements, Sc, Y, Zr, Ba, Hf and Th in geological samples by ICP-MS after Tm addition and alkaline fusion. Geostand. Geoanal. Res. 33, 51-62.

Bayon, G., Henderson, G.M., Bohn, M., 2009. U–Th stratigraphy of a cold seep carbonate crust. Chem. Geol. 260, 47-56.

Bayon, G., Birot, D., Ruffine, L., Caprais, J.C., Ponzevera, E., Bollinger, C., Donval, J.P., Charlou, J.L., Voisset, M., Grimaud, S., 2011a. Evidence for intense REE scavenging at cold seeps from the Niger Delta margin. Earth Planet. Sci. Lett. 312, 443-452.

Bayon, G., Birot, D., Bollinger, C., Barrat, J.A., 2011b. Multi-element determination of trace elements in natural water reference materials by ICP-SFMS after Tm addition and iron co-precipitation. Geostand. Geoanal. Res. 35, 145-153.

Bayon, G., Dupré, S., Ponzevera, E., Etoubleau, J., Chéron, S., Pierre, C., Mascle, J., Boetius, A., De Lange, G.J., 2013. Formation of carbonate chimneys in the Mediterranean Sea linked to deep-water oxygen depletion. Nat. Geosci. 6, 755-760.

Bayon, G. et al., 2015. Rare earth elements and neodymium isotopes in world river sediments revisited. Geochim. Cosmochim. Acta 170, 17-38.

Bayon, G., Lambert, T., Vigier, N., De Deckker, P., Freslon, N., Jang, K., Larkin, C.S., Piotrowski, A.M., Tachikawa, K., Thollon, M., Tipper, E.T., 2020. Rare earth element and neodymium isotope tracing of sedimentary rock weathering. Chem. Geol. 553, 119794.

Bergquist, D.C., Williams, F.M., Fisher, C.R., 2000. Longevity record for deep-sea invertebrate. Nature 403, 499-500.

Birgel, D., Feng, D., Roberts, H.H., Peckmann, J., 2011. Changing redox conditions at cold seeps as revealed by authigenic carbonates from Alaminos Canyon, northern Gulf of Mexico. Chem. Geol. 285, 82-96.

Boetius, A., 2005. Microfauna-macrofauna interaction in the seafloor: lessons from the tubeworm. PLoS Biol. 3, e102.

Boetius, A., Wenzhöfer, F., 2013. Seafloor oxygen consumption fuelled by methane from cold seeps. Nat. Geosci. 6, 725-734.

Borowski, W.S., Paull, C.K., Ussler III, W., 1996. Marine pore-water sulfate profiles indicate in situ methane flux from underlying gas hydrate. Geology 24, 655-658.

Bowen, H.J.M., 1966. Trace Elements in Biochemistry. Academic Press, London and New York.

Bright, M., Lallier, F.H., 2010. The biology of vestimentiferan tubeworms. Oceanogr. Mar. Biol. 48, 213-266.

Burdige, D. J., 1993. The biogeochemistry of manganese and iron reduction in marine sediments. Earth Sci. Rev. 35, 249-284.

Calvert, S.E., Pedersen, T.F., 1993. Geochemistry of recent oxic and anoxic marine sediments: implications for the geological record. Mar. Geol. 113, 67-88.

Catling, D.C., Zahnle, K.J., McKay, C.P., 2001. Biogenic Methane, Hydrogen Escape, and the Irreversible Oxidation of Early Earth. Science 293, 839-843.

Charlou, J. L. et al., 2004. Physical and chemical characterization of gas hydrates and associated methane plumes in the Congo–Angola Basin. Chem. Geol. 205, 405-425.

Chen, F., Hu, Y., Feng, D., Zhang, X., Cheng, S., Cao, J., Lu, H., Chen D., 2016. Evidence of intense methane seepages from molybdenum enrichments in gas hydrate-bearing sediments of the northern South China Sea. Chem. Geol. 443, 173–181.

Collin, P.Y., Kershaw, S., Tribovillard, N., Forel, M.B., Crasquin, S., 2015. Geochemistry of post-extinction microbialites as a powerful tool to assess the oxygenation of shallow marine water in the immediate aftermath of the end-Permian mass extinction. Int. J. Earth Sci. 104, 1025-1037.

Cordes E.E., Arthur M.A., Shea K., Fisher C.R., 2005. Modeling the mutualistic interactions between tubeworms and microbial consortia. PLoS Biol. 3, 497–506.

Cordes, E.E., Bergquist, D.C., Redding, M.L., Fisher, C.R., 2007. Patterns of growth in cold-seep vestimenferans including Seepiophila jonesi: a second species of long-lived tubeworm. Mar. Ecol. 28, 160-168.

Crémière, A. et al., 2016. Fluid source and methane-related diagenetic processes recorded in cold seep carbonates from the Alvheim channel, central North Sea. Chem. Geol. 432, 16-33.

Crespo-Medina, M. et al., 2014. The rise and fall of methanotrophy following a deepwater oil-well blowout. Nat. Geosci. 7, 423-427.

Crusius, J., Calvert, S., Pedersen, T., Sage, D., 1996. Rhenium and molybdenum enrichments in sediments as indicators of oxic, suboxic and sulfidic conditions of deposition. Earth Planet. Sci. Lett. 145, 65-78.

Della Porta, G., Webb, G.E., McDonald, I., 2015. REE patterns of microbial carbonate and cements from Sinemurian (Lower Jurassic) siliceous sponge mounds (Djebel Bou Dahar, High Atlas, Morocco). Chem. Geol. 400, 65-86.

Duperron, S. , De Beer, D., Zbinden, M., Boetius, A., Schipani, V., Kahil, N., Gaill, F., 2009. Molecular characterization of bacteria associated with the trophosome and the tube of *Lamellibrachia* sp., a siboglinid annelid from cold seeps in the eastern Mediterranean. FEMS Microbiol. Ecol. 69, 395-409.

Duperron, S., Gaudron, S.M., Lemaitre, N., Bayon, G., 2014. A microbiological and biogeochemical investigation of the cold seep tubeworm *Escarpia southwardae* (Annelida: Siboglinidae): Symbiosis and trace element composition of the tube. Deep Sea Res. Part I Oceanogr. 90, 105-114.

Durkin, A., Fisher, C.R., Cordes, E.E., 2017. Extreme longevity in a deep-sea vestimentiferan tubeworm and its implications for the evolution of life history strategies. Sci. Nat-Heidelberg 104, 63.

Feng, D., Roberts, H.H., 2010. Initial results of comparing cold-seep carbonates from mussel- and tubeworm-associated environments at Atwater Valley lease block 340, northern Gulf of Mexico. Deep-Sea Res. Part II-Top. Stud. Oceanogr. 57, 2030-2039.

Feng, D., Chen, D., Qi, L., Roberts, H.H., 2008. Petrographic and geochemical characterization of seep carbonate from Alaminos Canyon, Gulf of Mexico. Chin. Sci. Bull. 53, 1716-1724.

Feng, D., Chen, D., Roberts, H.H., 2009a. Petrographic and geochemical characterization of seep carbonate from Bush Hill (GC 185) gas vent and hydrate site of the Gulf of Mexico. Mar. Petrol. Geol. 26, 1190-1198.

Feng, D., Chen, D., Peckmann, J., 2009b. Rare earth elements in seep carbonates as tracers of variable redox conditions at ancient hydrocarbon seeps. Terr. Nova 21, 49-56.

Feng, D., Chen, D., Peckmann, J., Bohrmann, G., 2010. Authigenic carbonates from methane seeps of the northern Congo fan: microbial formation mechanism. Mar. Petrol. Geol. 27, 748-756.

Feng, D., Cordes, E.E., Roberts, H.H., Fisher, C.R., 2013. A comparative study of authigenic carbonates from mussel and tubeworm environments: Implications for discriminating the effects of tubeworms. Deep Sea Res. Part I Oceanogr. 75, 110-118.

Fitriyanto, N.A., Fushimi, M., Matsunaga, M., Pertiwiningrum, A., Iwama, T., Kawai, K., 2011. Molecular structure and gene analysis of Ce^{3+}-induced methanol dehydrogenase of *Bradyrhizobium* sp. MAFF211645. J. Biosci. Bioeng. 111, 613-617.

Flores, J.F., Fisher, C.R., Carney, S.L., Green, B.N., Freytag, J.K., Schaeffer, S.W., Royer, W.E., 2005. Sulfide binding is mediated by zinc ions discovered in the crystal structure of a hydrothermal vent tubeworm hemoglobin. Proc. Nat. Acad. Sci. 102, 2713-2718.

Franchi, F., Rovere, M., Gamberi, F., Rashed, H., Vaselli, O., Tassi, F., 2017. Authigenic minerals from the Paola Ridge (southern Tyrrhenian Sea): Evidences of episodic methane seepage. Mar. Petrol. Geol. 86, 228-247.

Freytag, J.K., Girguis, P.R., Bergquist, D.C., Andras, J.P., Childress, J.J., Fisher, C.R., 2001. A paradox resolved: sulfide acquisition by roots of seep tubeworms sustains net chemoautotrophy. Proc. Nat. Acad. Sci. 98, 13408-13413.

Gaill, F., Persson, J., Sugiyama, J., Vuong, R., Chanzy, H., 1992. The chitin system in the tubes of deep-sea hydrothermal vent worms. J. Struct. Biol. 109, 116-128.

Gaill, F., Shillito, B., Ménard, F., Goffinet, G., Childress, J.J., 1997. Rate and process of tube production by the deep-sea hydrothermal vent tubeworm Riftia pachyptila. Mar. Ecol. Prog. Ser. 148, 135-143.

Gieskes, J., Mahn, C., Day, S., Martin, J.B., Greinert, J., Rathburn, T., McAdoo, B., 2005. A study of the chemistry of pore fluids and authigenic carbonates in methane seep environments: Kodiak Trench, Hydrate Ridge, Monterey Bay, and Eel River Basin. Chem. Geol. 220, 329-345.

Glass, J.B., Orphan, V.J., 2012. Trace Metal Requirements for Microbial Enzymes Involved in the Production and Consumption of Methane and Nitrous Oxide. Front. Microbiol. 3, 61. doi:10.3389/fmicb.2012.00061.

Greinert, J., Bohrmann, G., Suess, E., 2001. Gas hydrate-associated carbonates and methane-venting at Hydrate Ridge: classification, distribution and origin of authigenic lithologies. Geophys. Monogr. Ser. 124, 99-114.

Haley, B.A., Klinkhammer, G.P., McManus, J., 2004. Rare earth elements in pore waters of marine sediments. Geochim. Cosmochim. Acta 68, 1265-1279.

Han, X., Suess, E., Huang, Y., Wu, N., Bohrmann, G., Su, X., Eisenhauer, A., Rehder, G., Fang, Y., 2008. Jiulong methane reef: microbial mediation of seep carbonates in the South China Sea. Mar. Geol. 249, 243-256.

Hilario, A., Capa, M., Dahlgren, T.G., Halanych, K.M., Little, C.T., Thornhill, D.J., Verna, C., Glover, A.G., 2011. New perspectives on the ecology and evolution of siboglinid tubeworms. PloS One 6(2).

Himmler, T., Bach, W., Bohrmann, G., Peckmann, J., 2010. Rare earth elements in authigenic methane-seep carbonates as tracers for fluid composition during early diagenesis. Chem. Geol. 277, 126-136.

Himmler, T., Haley, B.A., Torres, M.E., Klinkhammer, G.P., Bohrmann, G., Peckmann, J., 2013. Rare earth element geochemistry in cold-seep pore waters of Hydrate Ridge, northeast Pacific Ocean. Geo-Mar. Lett. 33, 369-379.

Himmler, T., Birgel, D., Bayon, G., Pape, T., Ge, L., Bohrmann, G., Peckmann, J., 2015. Formation of seep carbonates along the Makran convergent margin, northern Arabian Sea and a molecular and isotopic approach to constrain the carbon isotopic composition of parent methane. Chem. Geol. 415, 102-117.

Hu, Y., Feng, D., Peckmann, J., Roberts, H.H., Chen, D., 2014. New insights into cerium anomalies and mechanisms of trace metal enrichment in authigenic carbonate from hydrocarbon seeps. Chem. Geol. 381, 55-66.

Hu, Y., Feng, D., Liang, Q., Xia, Z., Chen, L., Chen, D., 2015. Impact of anaerobic oxidation of methane on the geochemical cycle of redox sensitive elements at cold-seep sites of the northern South China Sea. Deep-Sea Res. Part II-Top. Stud. Oceanogr. 122, 84–94.

International Atomic Energy Agency. MA-A-1/TM, trace elements in copepod homogenate. Reference sheet. IAEA, Monaco (1990).

Julian, D., Gaill, F., Wood, E., Arp, A.J., Fisher, C.R., 1999. Roots as a site of hydrogen sulfide uptake in the hydrocarbon seep vestimentiferan Lamellibrachia sp. J. Exp. Biol. 202, 2245-2257.

Joye, S.B., MacDonald, I.R., Leifer, I., Asper, V., 2011. Magnitude and oxidation potential of hydrocarbon gases released from the BP oil well blowout. Nat. Geosci. 4, 160-164.

Kamber, B.S., Webb, G.E., Gallagher, M., 2014. The rare earth element signal in Archaean microbial carbonate: information on ocean redox and biogenicity. J. Geol. Soc. 171, 745-763.

Kamber, B.S., Webb, G.E., 2001. The geochemistry of late Archaean microbial carbonate: implications for ocean chemistry and continental erosion history. Geochim. Cosmochim. Acta 65, 2509-2525.

Konhauser, K.O., Pecoits, E., Lalonde, S.V., Papineau, D., Nisbet, E.G., Barley, M.E., Arndt, N.T., Zahnle, K., Kamber, B.S., 2009. Oceanic nickel depletion and a methanogen famine before the Great Oxidation Event. Nature 458, 750-753.

Lawrence, M. G., Greig, A., Collerson, K.D., Kamber, B.S., 2006. Rare earth element and yttrium variability in South East Queensland waterways. Aquat. Geochem. 12, 39-72.

Lemaitre, N., Bayon, G., Ondréas, H., Caprais, J.C., Freslon, N., Bollinger, C., Rouget, M.L., De Prunelé, A., Ruffine, L., Olu-Le Roy, K., Sarthou, G., 2014. Trace element behaviour at cold seeps and the potential export of dissolved iron to the ocean. Earth Planet. Sci. Lett. 404, 376-388.

Maher, W. Forster, S., Krikowa, F., Snitch, P., Chapple, G., Craig, P., 2001. Measurement of trace elements and phosphorus in marine animal and plant tissues by low-volume microwave digestion and ICP-MS. Atom. Spectroscopy 22, 361-370.

Marcon, Y., Ondréas, H., Sahling, H., Bohrmann, G., Olu, K., 2014. Fluid flow regimes and growth of a giant pockmark. Geology 42, 63-66.

McManus, J., Berelson, W.M., Klinkhammer, G.P., Hammond, D.E., Holm, C., 2005. Authigenic uranium: relationship to oxygen penetration depth and organic carbon rain. Geochim. Cosmochim. Acta 69, 95-108.

Medina-Silva, R. et al., 2018. Microbiota associated with tubes of *Escarpia* sp. from cold seeps in the southwestern Atlantic Ocean constitutes a community distinct from that of surrounding marine sediment and water. Anton. Leeuw. Int. J. G. 111, 533-550.

Naehr, T. H., Eichhubl, P., Orphan, V. J., Hovland, M., Paull, C. K., Ussler III, W., Lorenson, T.D., Greene, H. G., 2007. Authigenic carbonate formation at hydrocarbon seeps in

continental margin sediments: a comparative study. Deep-Sea Res. Part II-Top. Stud. Oceanogr. 54, 1268-1291.

Nakagawa, T., Mitsui, R., Tani, A., Sasa, K., Tashiro, S., Iwama, T., Hayakawa, T., Kawai, K., 2012. A catalytic role of XoxF1 as La^{3+}-dependent methanol dehydrogenase in *Methylobacterium extorquens* strain AM1. PLoS One 7, e50480.

Novikova, S.A., Shnyukov, Y.F., Sokol, E.V., Kozmenko, O.A., Semenova, D.V., Kutny, V.A., 2015. A methane-derived carbonate build-up at a cold seep on the Crimean slope, north-western Black Sea. Mar. Geol. 363, 160-173.

Ochsner, A.M., Hemmerle, L., Vonderach, T., Nüssli, R., Bortfeld-Miller, M., Hattendorf, B., Vorholt, J.A., 2019. Use of rare-earth elements in the phyllosphere colonizer *Methylobacterium extorquens* PA1. Mol. Microbiol. 111, 1152-1166.

Olu-Le Roy, K., Caprais, J. C., Fifis, A., Fabri, M. C., Galéron, J., Budzinsky, H., Le Ménach, K., Khripounoff, A., Ondréas, H., Sibuet, M., 2007. Cold-seep assemblages on a giant pockmark off West Africa: spatial patterns and environmental control. Mar. Ecol. 28, 115-130.

Ondréas, H. et al., 2005. ROV study of a giant pockmark on the Gabon continental margin. Geo-Mar. Lett. 25, 281-292.

Peketi, A., Mazumdar, A., Joshi, R.K., Patil, D.J., Srinivas, P.L., Dayal, A.M., 2012. Tracing the Paleo sulfate-methane transition zones and H2S seepage events in marine sediments: An application of C-S-Mo systematics. Geochem. Geophys. Geosyst. 13, Q10007, doi:10.1029/2012GC004288.

Picone, N., Op den Camp, H.J., 2019. Role of rare earth elements in methanol oxidation. Curr. Opin. Chem. Biol. 49, 39–44.

Pierre, C., Bayon, G., Blanc-Valleron, M.M., Mascle, J., Dupré, S., 2014. Authigenic carbonates related to active seepage of methane-rich hot brines at the Cheops mud volcano,

Menes caldera (Nile deep-sea fan, eastern Mediterranean Sea). Geo-Mar. Lett. 34, 253-267.

Planavsky, N., Bekker, A., Rouxel, O.J., Kamber, B., Hofmann, A., Knudsen, A., Lyons, T. W., 2010. Rare earth element and yttrium compositions of Archean and Paleoproterozoic Fe formations revisited: new perspectives on the significance and mechanisms of deposition. Geochim. Cosmochim. Acta 74, 6387-6405.

Pol, A., Barends, T.R.M., Dietl, A., Khadem, A.F., Eygensteyn, J., Jetten, M.S.M., Op den Camp, H.J.M., 2014. Rare earth metals are essential for methanotrophic life in volcanic mudpots. Environ. Microbiol. 16, 255–264.

Pop Ristova, P., Wenzhofer, F., Ramette, A., Zabel, M., Fischer, D., Kasten, S., Boetius, A., 2012. Bacterial diversity and biogeochemistry of different chemosynthetic habitats of the REGAB cold seep (West African margin, 3160 m water depth). Biogeosciences 9, 5031-5048.

Rincón-Tomás, B., González, F.J., Sonnza, L., Sauter, K., Madureira, P., Medialdea, T., Carlsson, J., Reitner, J., Hoppert, M., 2020. Siboglinidae Tubes as an Additional Niche for Microbial Communities in the Gulf of Cádiz—A Microscopical Appraisal. Microorganisms 8, 367

Rongemaille, E., Bayon, G., Pierre, C., Bollinger, C., Chu, N.C., Fouquet, Y., Riboulot, V., Voisset, M., 2011. Rare earth elements in cold seep carbonates from the Niger delta. Chem. Geol. 286, 196–206.

Sato, H., Hayashi, K.I., Ogawa, Y., Kawamura, K., 2012. Geochemistry of deep sea sediments at cold seep sites in the Nankai Trough: Insights into the effect of anaerobic oxidation of methane. Mar. Geol. 323–325.

Schier, K., Bau, M., Muenker, C., Beukes, N., Viehmann, S., 2018. Trace element and Nd isotope composition of shallow seawater prior to the Great Oxidation Event: Evidence

from stromatolitic bioherms in the Paleoproterozoic Rooinekke and Nelani Formations, South Africa. Precambrian Res. 315, 92-102.

Schulz, H. D., Dahmke, A., Schinzel, U., Wallmann, K., Zabel, M., 1994. Early diagenetic processes, fluxes, and reaction rates in sediments of the South Atlantic. Geochim. Cosmochim. Acta 58, 2041-2060.

Semrau, J.D., DiSpirito, A.A., Gu, W., Yoon, S., 2018. Metals and methanotrophy. Appl. Environ. Microbiol. 84, e02289-17.

Shiller, A.M., Chan, E.W., Joung, D.J., Redmond, M.C., Kessler, J.D., 2017. Light rare earth element depletion during Deepwater Horizon blowout methanotrophy. Sci. Rep. 7, 10389.

Sholkovitz, E.R., Piepgras, D.J., Jacobsen, S.B., 1989. The pore water chemistry of rare earth elements in Buzzards Bay sediments. Geochim. Cosmochim. Acta 53, 2847-2856.

Sibuet, M., Olu, K., 1998. Biogeography, biodiversity and fluid dependence of deep-sea cold-seep communities at active and passive margins. Deep-Sea Res. Part II-Top. Stud. Oceanogr. 45, 517-567.

Skovran, E., Martinez-Gomes, N.C., 2015. Just add lanthanides. Science 348, 862-863

Smrzka, D., Zwicker, J., Klügel, A., Monien, P., Bach, W., Bohrmann, G., Peckmann, J., 2016. Establishing criteria to distinguish oil-seep from methane-seep carbonates. Geology 44, 667-670.

Smrzka, D., Zwicker, J., Misch, D., Walkner, C., Gier, S., Monien, P., Bohrmann, G., Peckmann, J., 2019. Oil seepage and carbonate formation: A case study from the southern Gulf of Mexico. Sedimentology 66, 2318-2353.

Smrzka, D., Zwicker, J., Bach, W., Feng, D., Himmler, T., Chen, D., Peckmann, J., 2019. The behavior of trace elements in seawater, sedimentary pore water, and their incorporation into carbonate minerals: a review. Facies 65, 41.

Smrzka, D., Feng, D., Himmler, T., Zwicker, J., Hu, Y., Monien, P., Tribovillard, N., Chen, D., Peckmann, J., 2020. Trace elements in methane-seep carbonates: Potentials, limitations, and perspectives. Earth Sci. Rev. 208, 103263.

Taubert, M., Grob, C., Howat, A.M., Burns, O.J., Dixon, J.L., Chen, Y., Murrell, J.C., 2015. XoxF encoding an alternative methanol dehydrogenase is widespread in coastal marine environments. Environ. Microbiol. 17, 3937-3948.

Teichert, B. M., Bohrmann, G., Suess, E., 2005. Chemoherms on Hydrate Ridge—Unique microbially-mediated carbonate build-ups growing into the water column. Palaeogeog. Palaeoclimatol. Palaeoecol. 227, 67-85.

Tong, H., Chen, D., 2012. First discovery and characterizations of late Cretaceous seep carbonates from Xigaze in Tibet, China. Chin. Sci. Bull. 57, 4363-4372.

Tribovillard, N., Algeo, T.J., Lyons, T., Riboulleau, A., 2006. Trace metals as paleoredox and paleoproductivity proxies: an update. Chem. Geol. 232, 12-32.

Tribovillard, N., Du Châtelet, E.A., Gay, A., Barbecot, F., Sansjofre, P., Potdevin, J.L., 2013. Geochemistry of cold seepage-impacted sediments: per-ascensum or per-descensum trace metal enrichment?. Chem. Geol. 340, 1-12.

Tyler, G., 2004. Rare earth elements in soil and plant systems – A review. Plant Soil 267, 191-206.

Wang, S., Magalhães, V.H., Pinheiro, L.M., Liu, J., Yan, W., 2015. Tracing the composition, fluid source and formation conditions of the methane-derived authigenic carbonates in the Gulf of Cadiz with rare earth elements and stable isotopes. Mar. Petrol. Geol. 68, 192-205.

Wang, S., Yan, W., Chen, Z., Zhang, N., Chen, H., 2014. Rare earth elements in cold seep carbonates from the southwestern Dongsha area, northern South China Sea. Mar. Petrol. Geol. 57, 482-493.

Wang, X., Bayon, G., Kim, J.H., Lee, D.H., Kim, D., Guéguen, B., Rouget, M.L., Barrat, J.A., Toffin, L., Feng, D., 2019. Trace element systematics in cold seep carbonates and associated lipid compounds. Chem. Geol. 528, 119277.

Wang, X., Barrat, J.A., Bayon, G., Chauvaud, L., Feng, D., 2020. Lanthanum anomalies as fingerprints of methanotrophy. Geochem. Perspect. Lett. (in press).

Yang, K., Chu, F., Zhu, Z., Dong, Y., Yu, X., Zhang, W., Ma, W., 2018. Formation of methane-derived carbonates during the last glacial period on the northern slope of the South China Sea. J. Asian Earth Sci. 168, 173-185.

Zhu, B., Ge, L., Yang, T., Jiang, S., Lv, X., 2019. Stable isotopes and rare earth element compositions of ancient cold seep carbonates from Enza River, northern Apennines (Italy): Implications for fluids sources and carbonate chimney growth. Mar. Petrol. Geol. 109, 434-448.

Zwicker, J., Smrzka, D., Himmler, T., Monien, P., Gier, S., Goedert, J.L., Peckmann, J., 2018. Rare earth elements as tracers for microbial activity and early diagenesis: A new perspective from carbonate cements of ancient methane-seep deposits. Chem. Geol. 501, 77-85.

Figure captions

Figure 1. **(a)** Seafloor photographs of bushes of siboglinid tubeworms (*Escarpia southwardae*) at the Regab pockmark. **(b)** The chitin-rich tube of *Escarpia southwardae* investigated in this study, with location of the sections analysed for trace elements.

Figure 2. Concentration profiles for selected trace elements (µg/g or ng/g), La and Ce anomalies, and shale-normalized La/Gd ratios along the tube. The anterior part of the tube

(from sections S1 to S8) corresponds to a redox front between ambient oxic seawater and the branchial plume region, characterized by oxygen-depleted conditions (horizontal orange band). The part of the tube between sections S1 and S44 was bathed by bottom water, while sections S44 to S55 correspond to the root-like posterior extension buried in the anoxic sediment. The second redox front between sections S44 to S49 corresponds to the seawater-sediment interface (horizontal orange band). The vertical grey shaded areas indicate the range of $(La/Gd)_N$, La and Ce anomalies in bottom waters at Regab (Lemaitre et al., 2014). The dashed lines correspond to La/La* and Ce/Ce* = 1, which indicate the absence of any La and Ce anomalies, respectively. Note that Mn and Fe concentrations are from Duperron et al. (2014).

Figure 3. Shale-normalized (WRAS) REE patterns for the studied siboglinid tube between (**a**) sections S1 and S8, (**b**) sections S9-S21, and (**c**) sections S22-S44 and S45-S55. (**d**) Also shown for comparison are the average REE patterns for Regab bottom waters (Lemaitre et al., 2014), together with global seawater and pore waters having shale-normalized Gd/Yb ratio >1 (considered as representative of anoxic pore waters). The references used for the global compilation of seawater and pore water data are listed in Supplementary Tables S1 and S2. Note that the tube samples from sections S22-S44 (black circles) and S45-S55 (blue squares) display REE patterns typical ambient bottom waters at the Regab pockmark and anoxic pore waters, respectively. In contrast, samples from sections S8-S21 (orange triangles) and S3-S7 (red diamonds) are characterized by pronounced La enrichments and the absence of Ce anomalies. The observed flat shale-normalized patterns for sections S1 and S2 reflect the presence of detrital sediment particles.

Figure 4. Relationship between Ce and La anomalies in studied siboglinid tube sections. The other REE data used for comparison include a global compilation of Ce/Ce* and La/La* for seawater and pore water (Tables S1 and S2), bottom waters at the Regab pockmark (Lemaitre et al., 2014) collected just above the seafloor (<1 m absf) and in the overlying water column (>1 m absf) (Lemaitre et al., 2014), and the Fe-Mn oxyhydroxide fraction extracted from Congo fan seafloor sediment (yellow star; Bayon et al., 2004). The tube sections from the buried posterior extension between sections S45-S55 plot within the field of pore waters (expect for S51 and S52), while the sections S22-S44 plot between the fields for pore waters and ambient bottom waters at Regab. In contrast, most of the sections from the anterior part of the tube display clear La enrichments that depart from expected pore water and seawater signatures.

Figure 5. Relationships between light-REE and Cu in the siboglinid tube sections. (**a**) La/Th vs Cu/Th. (**b**) La/La* vs Cu/Th. (**c**) Ce/Th vs Cu/Th. (**d**) Ce/Ce* vs Cu/Th. The observed co-enrichments of Cu, La and (to a lesser extent) Ce and in the anterior portion of the tube are interpreted as reflecting their uptake by aerobic methane-oxidising bacteria, as metalloenzymes catalyzing the transformation of methane to methanol, and methanol to formaldehyde, respectively.

Figure 6. Revisiting REE systematics in modern cold seep carbonates using (**a**) Ce/Ce* vs La/La* and (**b**) $(La/Gd)_N$ vs $(Gd/Yb)_N$ relationships. The REE data and references used for the compilation of cold seep carbonates are listed in Table S3. Most cold seep carbonates overlap with pore waters, except for some seafloor aragonite-rich chemoherms displaying particular La enrichments, as inferred from high $(La/Gd)_N$ (> ~ 0.8). These LREE enrichments are interpreted here as possibly reflecting the signature of REE-dependent methanotrophic

activity at the seafloor. Also shown for comparison are average laser-ablation data for pure aragonite in seep carbonates from the Makran accretionary prism (Himmler et al., 2010), in seep carbonates influenced by oil seepage in the Gulf of Mexico (Smrzka et al., 2019), and in ancient Phanerozoic seep carbonates (Zwicker et al., 2018).

The authors declare that they have no known competing financial interests or personal relationships that could have appeared to influence the work reported in this paper.

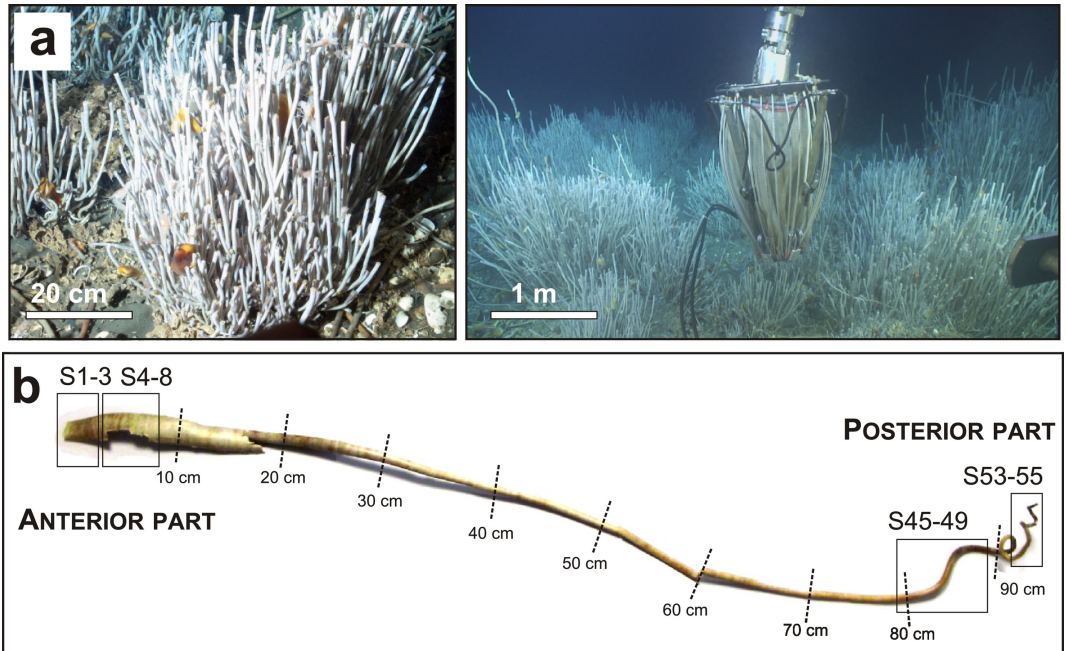
a
20 cm
1 m
b
S1-3 S4-8
ANTERIOR PART
POSTERIOR PART
S53-55
S45-49
10 cm
20 cm
30 cm
40 cm
50 cm
60 cm
70 cm
80 cm
90 cm

Figure 1

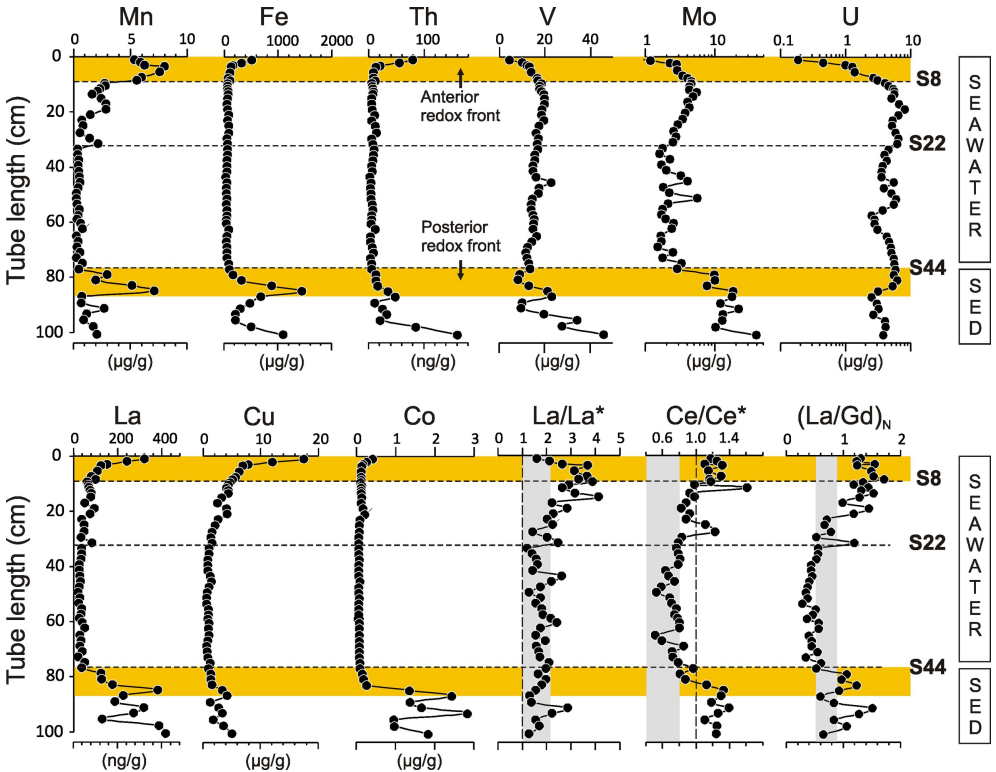
Mn
Fe
Th
V
Mo
U
La
Cu
Co
La/La*
Ce/Ce*
(La/Gd)N
Tube length (cm)
Anterior redox front
Posterior redox front
S8
S22
S44
SEAWATER
SED
(µg/g)
(ng/g)

Figure 2

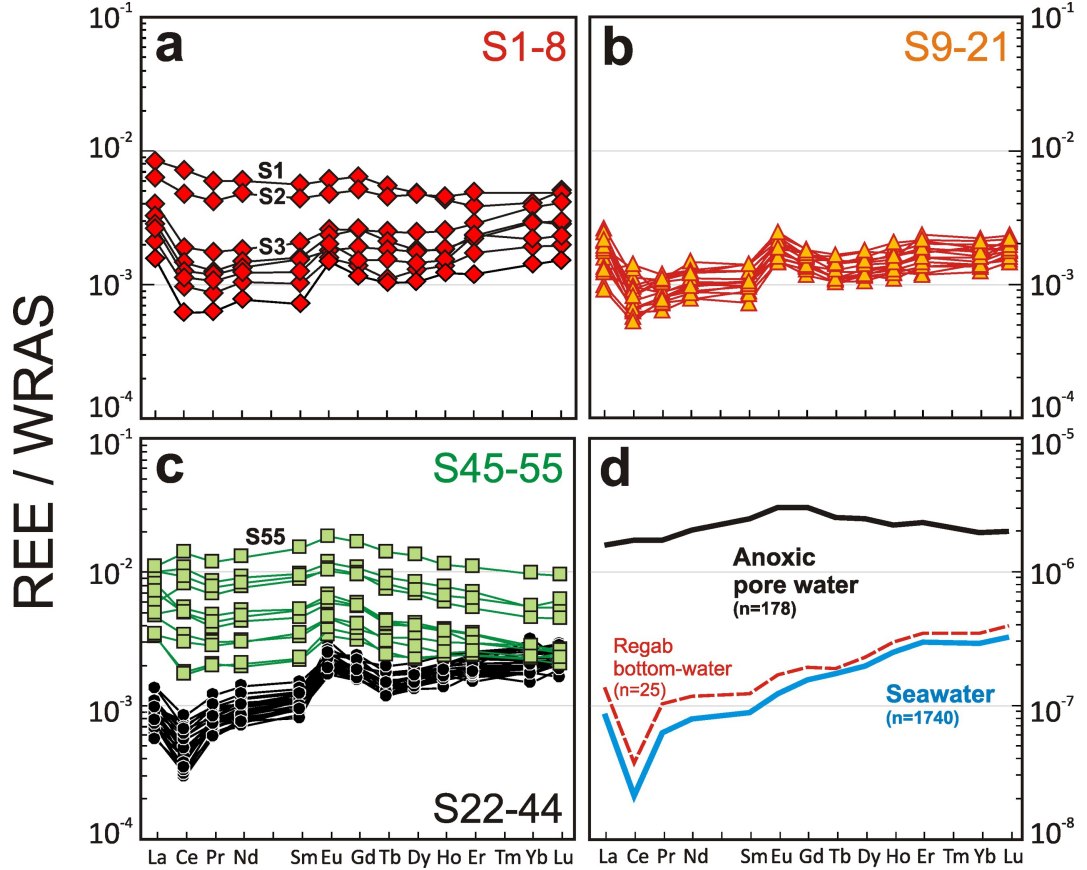
REE / WRAS
a
S1-8
S1
S2
S3
b
S9-21
c
S45-55
S55
S22-44
d
Anoxic
pore water
(n=178)
Regab
bottom-water
(n=25)
Seawater
(n=1740)
La Ce Pr Nd Sm Eu Gd Tb Dy Ho Er Tm Yb Lu

Figure 3

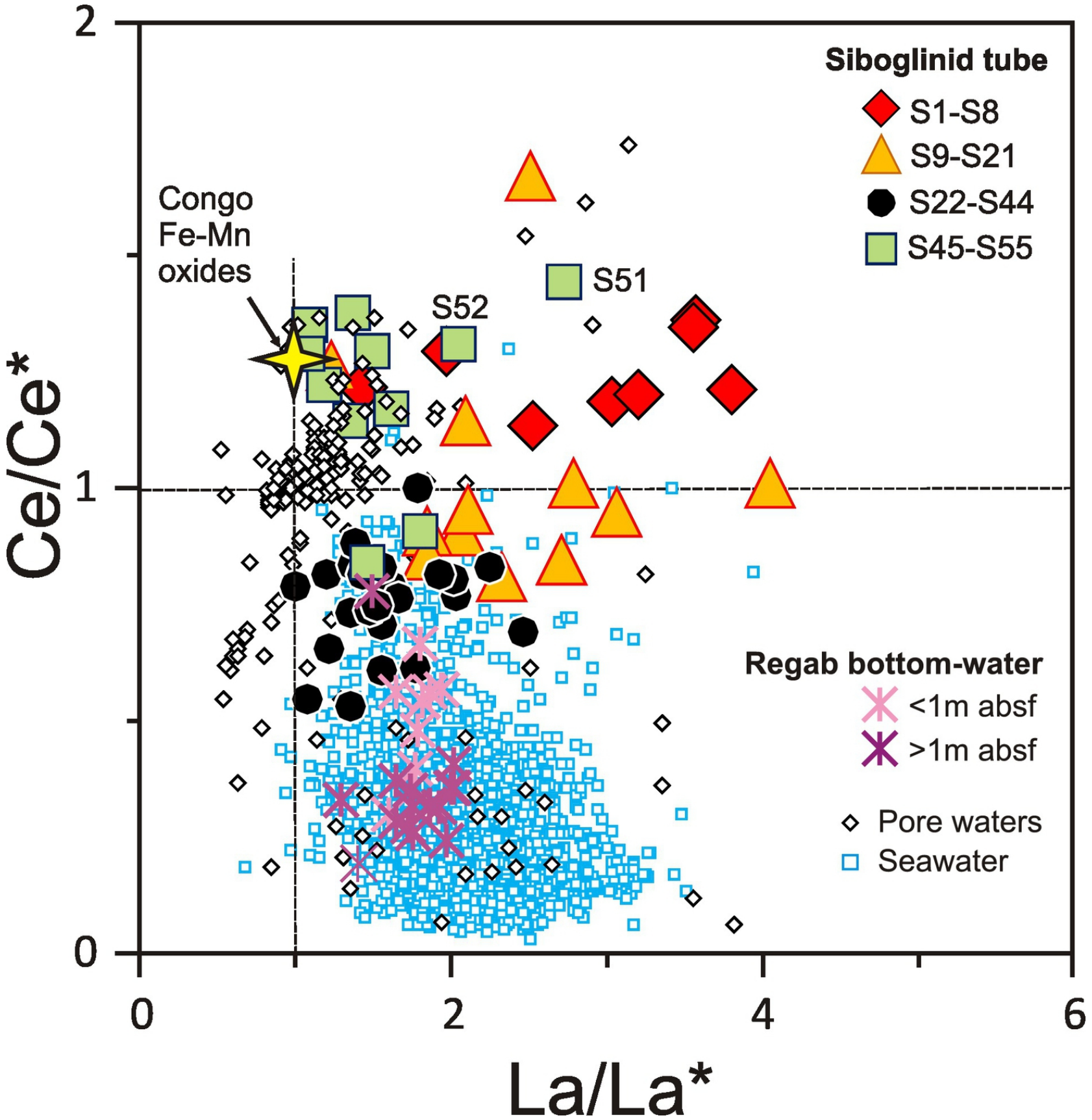
Siboglinid tube
S1-S8
S9-S21
S22-S44
S45-S55
Congo
Fe-Mn
oxides
S51
S52
Regab bottom-water
<1m absf
>1m absf
Pore waters
Seawater
Ce/Ce*
La/La*
0
1
2
0
2
4
6

Figure 4

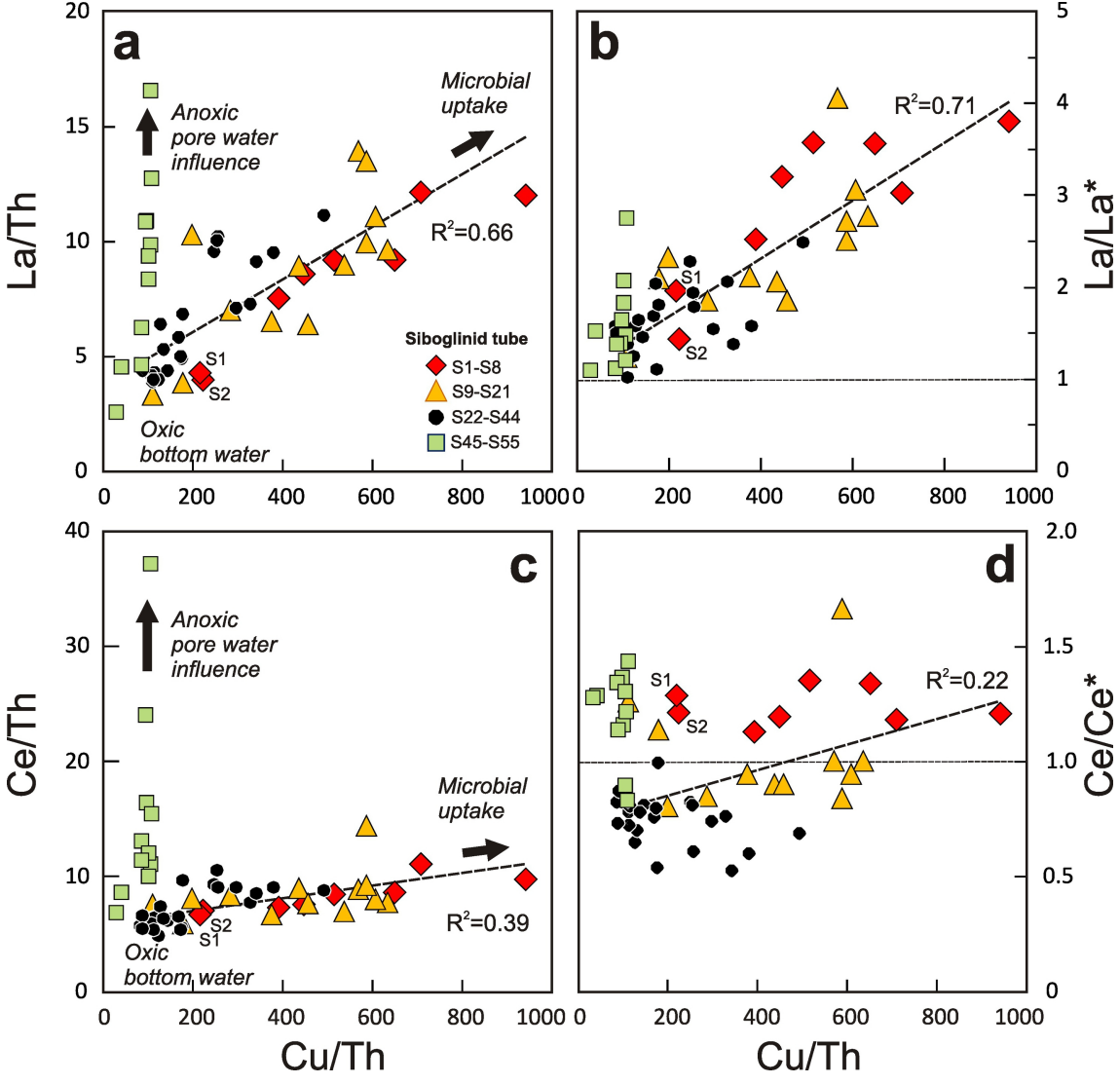
a
Anoxic
pore water
influence
Microbial
uptake
R²=0.66
Siboglinid tube
S1-S8
S9-S21
S22-S44
S45-S55
S1
S2
Oxic
bottom water
La/Th
b
R²=0.71
La/La*
c
Anoxic
pore water
influence
Microbial
uptake
R²=0.39
Oxic
bottom water
Ce/Th
Cu/Th
d
R²=0.22
Ce/Ce*
Cu/Th

Figure 5

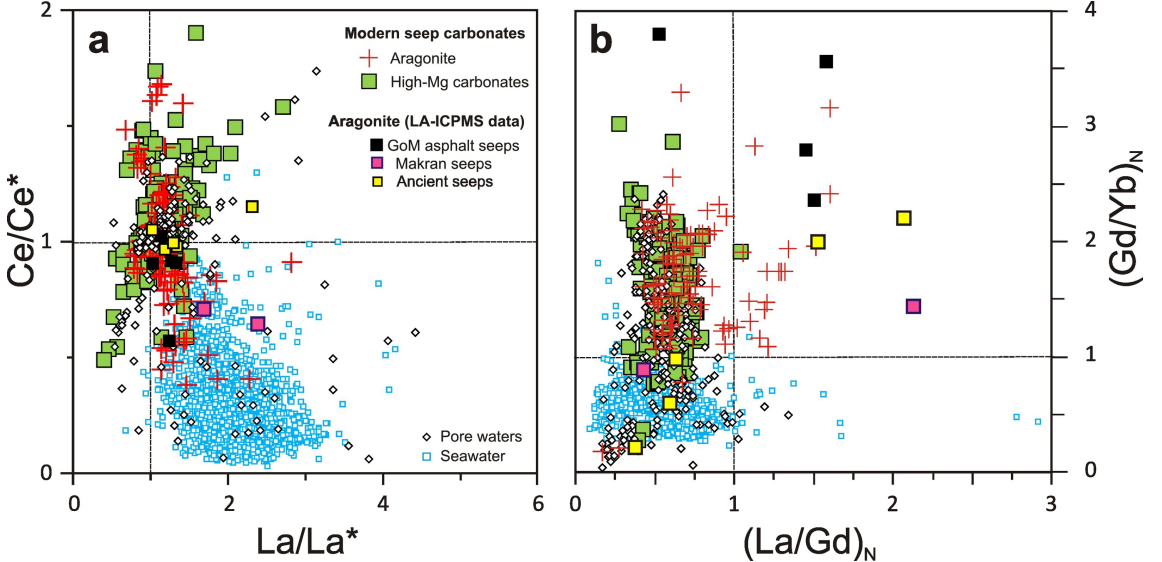
a
Modern seep carbonates
Aragonite
High-Mg carbonates
Aragonite (LA-ICPMS data)
GoM asphalt seeps
Makran seeps
Ancient seeps
Pore waters
Seawater
Ce/Ce*
La/La*
b
(La/Gd)N
(Gd/Yb)N

Figure 6